Quaternary Research 80 (2013) 510–521

Contents lists available at ScienceDirect

Quaternary Research

journal homepage: www.elsevier.com/locate/yqres

Isotope and trace element evolution of the Naica aquifer (Chihuahua, Mexico) over the past 60,000 yr revealed by speleothems

Fernando Gázquez [a,b,*], José-María Calaforra [a], Heather Stoll [c], Laura Sanna [d], Paolo Forti [e], Stein-Erik Lauritzen [f], Antonio Delgado [g], Fernando Rull [b], Jesús Martínez-Frías [b,h]

[a] Water Resources and Environmental Geology, University of Almería, Crta. Sacramento s/n, 04120, La Cañada de San Urbano, Almería, Spain
[b] Unidad Asociada UVA-CSIC al Centro de Astrobiología, University of Valladolid, Parque Tecnológico Boecillo, 47151 Valladolid, Spain
[c] Department of Geology, University of Oviedo, Arias de Velasco s/n, 30005 Oviedo, Spain
[d] Dipartimentpo di Scienze della Natura e del Territorio, Università degli Studi di Sassari, Via Piandanna 4, 07100 Sassari, Italy
[e] Department of Earth and Environmental Sciences, University of Bologna, Via Zamboni 67, 40126 Bologna, Italy
[f] Department of Earth Sciences, University of Bergen, Allégaten 41, N-5007 Bergen, Norway
[g] Instituto Andaluz de Ciencias de la Tierra, Camino del Jueves s/n, 18100 Armilla, Granada, Spain
[h] Geosciences Institute, IGEO (CSIC-UCM), Facultad de Ciencias Geológicas, C/ José Antonio Novais, 2, Ciudad Universitaria, 28040, Madrid, Spain

ARTICLE INFO

Article history:
Received 18 December 2012
Available online 22 October 2013

Keywords:
Cave minerals
Gypsum water of crystallization
Gypsum speleothems
Naica caves
Paleogroundwater
Selenite

ABSTRACT

The "espada" speleothems of Cueva de las Espadas (Naica Mine, Chihuahua, Mexico) comprise a high-purity selenite core overlain by successive deposits of calcite, gypsum and aragonite. Gypsum precipitated under water from a hydrothermal solution (~58°C) when the water table was above the cave level ca. 57 ka, during the last glaciation, and some intervals during deglaciation and the Holocene. Aragonite was deposited at lower temperatures (~26°C) in a perched lake occupying the cave bottom, when the water table dropped below the cave level during brief dry intervals during deglaciation and the early Holocene. The isotopic composition of gypsum water of crystallization shows that the deglaciation–Holocene aquifer water was enriched in deuterium by 12.8–8.7‰ relative to water from the last glaciation. This is attributed to an increased relative moisture contribution from the Gulf of Mexico during deglaciation and the Holocene compared to the last glaciation. This indicates that drier conditions occurred in the Naica area during the Holocene than around 57 ka. Furthermore, trace element analyses of gypsum served to deduce the circulation regime of the Naica aquifer during the past 60,000 yr, and also suggest that higher aquifer recharge occurred during the last glaciation.

Introduction and geological setting

Since the middle of the 19th century the Naica mining district, located in Chihuahua State, northern Mexico, has been one of the most important lead and silver producing areas in the world (Fig. 1A). At the Naica mine, zinc and lead sulfides enriched in silver are extracted (Alva-Valdivia et al., 2003). The regional stratigraphy comprises limestone and dolostone with interbedded clays and silts (Albian and Cenomanian) (Franco-Rubio, 1978). Intrusive magmatic activity during the Tertiary is evidenced by felsic dikes in the carbonate series (Megaw et al., 1988) (Fig. 1A). In fact, this part of the North American subcontinent is characterized by felsic dikes some 26.0–30.2 Ma old within the carbonate sequences (Alva-Valdivia et al., 2003). In the case of the Sierra de Naica, the intrusions penetrate an old northwest–southeast fracture. The dikes consist of calc-silicates with disseminated sulfides, as well as massive sulfides with sparse calc-silicates (Ruiz et al., 1986).

The contact between these igneous bodies and the groundwater created a hydrothermal system of brines, which flowed along the alignment of the dikes following lines of weakness (Ruiz et al., 1986). The oxidation of sulfide minerals gave rise to sulfates and metals in solution. Acidification due to this mechanism led to corrosion of the carbonate sequence and enabled the genesis of caves (Forti, 2010).

The mineralization process was long and characterized by three different phases (Erwood et al., 1979) corresponding to different chemical compositions and temperatures of the uplifting fluids. The conditions of early ore deposition were estimated (using fluid inclusion constraints) to be about 400–500°C and 100–270 MPa (Megaw et al., 1988). During this stage the skarn-bearing, chimney-manto, limestone replacement deposits were developed. The second phase was characterized by a temperature range between 240 and 490°C. In this stage hedenbergite–quartz–calcite was formed followed by galena sphalerite and chalcopyrite. During the final mineralization stage, when the thermal fluids got colder (119–379°C), calcite, anhydrite and quartz formed veins within the ore bodies (Erwood et al., 1979; Marín-Herrera et al., 2006). Hydrothermal anhydrite lenses are abundant in the carbonate sequence below the −240 m level (Forti, 2010). During a more recent stage (over the past 250 ka; Sanna et al., 2010), gypsum precipitation occurred at lower temperature (58°C; Garofalo et al., 2010), similar to the current temperature of the aquifer (52–54°C).

* Corresponding author.
E-mail address: f.gazquez@ual.es (F. Gázquez).

0033-5894/$ – see front matter © 2013 University of Washington. Published by Elsevier Inc. All rights reserved.
http://dx.doi.org/10.1016/j.yqres.2013.09.004

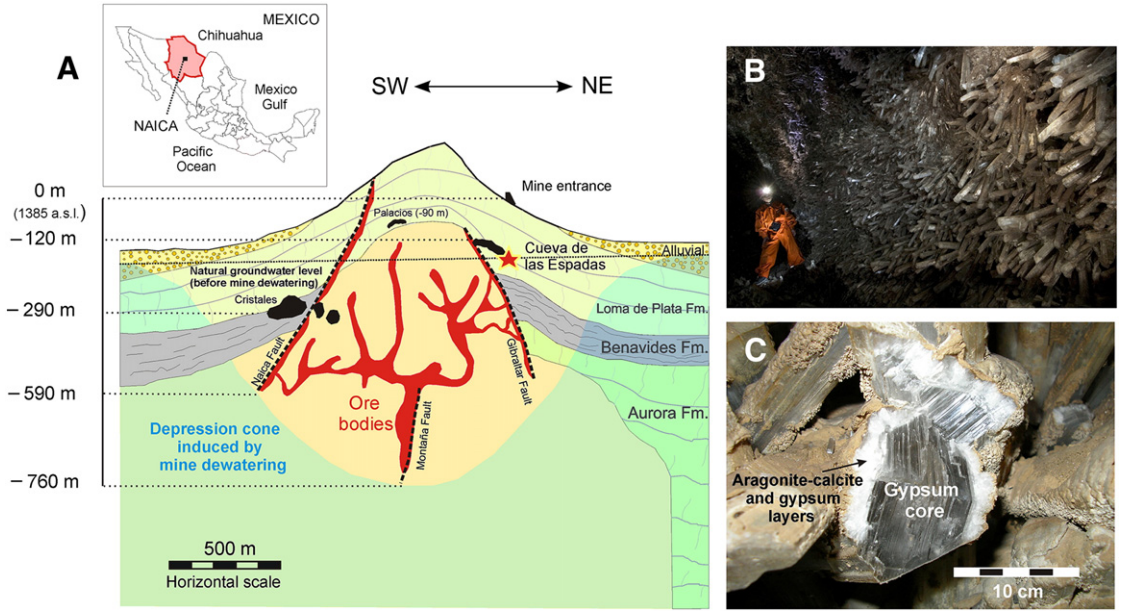

Figure 1. Location of Cueva de las Espadas within the Naica mine complex (27°51′01″N, 105°29′39″W, 1265 m asl). A. Sketch of the Naica mine with the locations of the main natural caves discovered. The natural groundwater level of the Naica aquifer (130–140 m below the mine entrance) and that induced by the mine dewatering at the current time (800 m below the mine entrance) are represented; B. The espada speleothems consist of a prismatic gypsum crystal covered by several layers of carbonates and microcrystalline gypsum; C. The speleothem, already broken through vandalism, was taken from the floor of Cueva de las Espadas.

From a hydrogeological point of view, the Naica aquifer consists of a subhorizontal carbonate sequence up to 3000 m deep, whose thickness decreases towards the mountains of Pajarillos (to the south), Camargo (southeast) and El Alamillo (north), all of which lie around 20 km from the Sierra de Naica (Giulivo et al., 2007). Previous hydrogeological studies suggested that allogenic feed to the Naica aquifer from the Conchos and San Pedro rivers (~40 km from the Sierra de Naica) are quite low (Giulivo et al., 2007). The drawdown cone produced by the pumping that keeps the mine dewatered – a necessity when such deep ore bodies are being exploited – means that the water table around the Naica mine currently lies at more than 800 m depth. Nonetheless, the natural groundwater level (with no water pumping) would lie 130–140 m below the mine entrance (Fig. 1A) (Giulivo et al., 2007).

Highly unusual speleothems occur in many caves within this hypogenic karst system, such as in "Cueva de los Cristales" (Crystals Cave) (Marín-Herrera et al., 2006; García-Ruiz et al., 2007; Forti, 2010), "Ojo de la Reina" (Queen's Eye Cave) (Forti, 2010; Badino et al., 2011) and "Cueva de las Velas" (Sails Cave) (Bernabei et al., 2007) (Fig. 2), all of them 290 m below the mine entrance (170 m below the current natural groundwater level; Fig. 1A). The "Cueva de los Palacios" (Palace Cave) was the last cave discovered in the Naica mine, 90 m below the mine entrance (40 m above the natural groundwater level; Beverly and Forti, 2010). In this cave, there is no trace of euhedral gypsum crystals, although gypsum crust flowers and gypsum-hair do occur. This is evidence that this cave used to lie only a few meters above the water table, where capillary uplift and evaporation of water into its atmosphere could occur.

The Cueva de las Espadas (Cave of Swords), situated 120 m below the mine entrance (Foshag, 1927; Rickwood, 1981; Gázquez et al., 2012), hosts a rare kind of speleothem, the espada speleothems (Figs. 1B, C and 2A), which are the focus of this paper.

The entrance to the Cueva de las Espadas follows subvertical fractures connected to the Montaña Fault. The difference in height between

Figure 2. The three main caves in the Naica mine. A. Cueva de las Espadas (−120 m), gallery from which the speleothems were sampled; B. Cueva de los Cristales (−290 m) with selenite crystals up to 11 m in length (photo by La Venta Exploring Team); C. Cueva del Ojo de la Reina (−290 m) which houses gypsum crystals with hydromagnesite and calcite alteration crusts (note: depths relative to the mine entrance level).

https://doi.org/10.1016/j.yqres.2013.09.004 Published online by Cambridge University Press

the cave entrance and its base is 20 m; when it was discovered in 1910, the cave entrance was completely covered by selenite crystals up to 2 m long (Foshag, 1927; Rickwood, 1981). Uncontrolled pillaging meant that, today, many of these crystals are held in private collections or in museum exhibits.

At present, water in the Cueva de las Espadas is quite scarce and limited to condensation water on the walls and surfaces of the speleothems. This mine level has kept in the vadose zone of the aquifer at least from 1950, when the mine dewatering produced by the pumping started (Giulivo et al., 2007).

Nonetheless, the presence of euhedral selenite crystals and subaqueous aragonite concretions in the deepest part of the cave is clear evidence of phreatic conditions in the past (as suggested by Forti, 2010; Gázquez et al., 2012, and also discussed in the current paper). In fact, Gázquez et al. (2012) proposed a model for the genesis of these speleothems, whereby the gypsum was precipitated under phreatic conditions when the cave was totally submerged below the water table. However, during certain periods the water table dropped beneath the level of the cave and under these circumstances vadose conditions predominated in the upper cave level. Meanwhile, subaqueous aragonite precipitation occurred in a cave pool occupying the lower level of Cueva de las Espadas.

In the current article, the mineralogy and the geochemistry (stable isotopes and trace elements) of the espada speleothems are examined in order to shed light on their origin. In addition, geochemical data provide a discontinuous record of changes in the characteristics (temperature and salinity) of the Naica aquifer water at the Cueva de las Espadas level during the past 60 ka, linked to climate changes that took place in northern Mexico over the transition between the last glaciation and the Holocene.

Methodology

Sampling method

Subsamples for mineralogical and geochemical analyses were extracted from an already-broken espada speleothem collected from the floor of the Cueva de las Espadas. The speleothem, approximately 15 cm long and 6 cm in diameter, displays a brownish coating that has also been observed on the speleothems from the lower part of the cave walls, whereas crystals more than 2 m above the cave floor are completely clear and transparent. This fact suggests that the analyzed speleothem formed in the lower part of the cave.

A slice of the espada speleothem was cut perpendicular to its principal growth axis (plane 010) and perpendicular to the exfoliation plane of gypsum, 10 cm from its upper tip. The rest of the speleothem was cut to the main crystallographic axis of the gypsum crystal. Powdered subsamples were then drilled using a Dremel drill with a 0.8 mm diameter bit, as shown in Figure 3.

Nineteen carbonate subsamples were analyzed for $\delta^{13}C$ and $\delta^{18}O$, and 33 gypsiferous subsamples were analyzed for δD of water of crystallization and trace element content. Two powdered subsamples of the aragonite layers of the espada speleothem were dated by U–Th analysis. Furthermore, one powdered gypsum subsample was extracted from selenite core of the speleothem. To obtain the ≤10 g of gypsum necessary for U–Th analysis, practically the whole gypsum core had to be crushed (Fig. 3).

Raman spectroscopy and EDX mapping

The mineralogy was determined by micro-Raman spectroscopy on a polished lamina (100 μm) longitudinal to the main crystallographic axis of the inner gypsum crystal (Fig. 4A). This technique enabled thin mineral layers of the speleothems to be analyzed. The spectrometer used was a KOSI HoloSpec f/1.8i model from Kaiser. Microanalyses up to a 5 μm diameter spot were undertaken with a Nikon Eclipse E600 microscope (Gázquez et al., 2012). The Raman vibration bands overlap those identified in previous work on gypsum (Berenblut et al., 1971), calcite (Rutt and Nicola, 1974) and aragonite (Frech et al., 1980). Raman analyses were performed at the Unidad Asociada UVA-CSIC-CAB of the University of Valladolid (Spain). EDX (Energy-Dispersive X-ray spectroscopy) was used for sulfur mapping acquisition on the same polished lamina as described by Gázquez et al. (2012).

Isotope analysis methods

δD of gypsum water of crystallization

Powdered gypsum subsamples (0.6 mg) were analyzed for δD of the water of crystallization using the silver encapsulation method (Sauer et al., 2009), which consists of high-temperature pyrolysis of the samples in a graphite reactor (at 1450°C) and isotopic measurement of the H_2 generated. Before analysis, hygroscopic water was removed by pumping the sample in a vacuum for 3 h at room temperature with a liquid nitrogen trap fitted on the pumping line to remove absorbed water from the gypsum. This low-vacuum pumping (10^{-3} mbar) was found to be an effective method to remove absorbed water with no detectable loss of water of crystallization (Playá et al., 2005). The δD values of the gypsum samples were measured using a TC/EA coupled to an IRMS (Isotopic Ratio Mass Spectrometer) Delta Plus XL (Thermo Finnigan). Samples were prepared and analyzed in triplicate. This method, unlike others

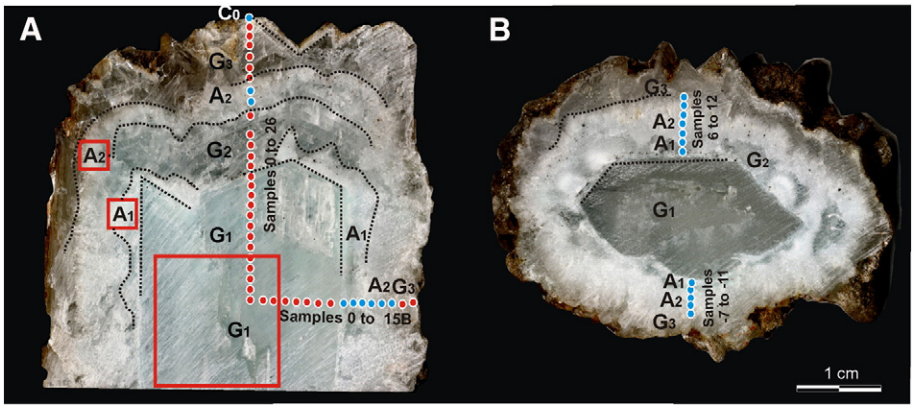

Figure 3. Sampling along a longitudinal section to the axis of an espada speleothem (A), and along a perpendicular section (B). The composition in trace elements was analyzed, as well as the isotope composition (δD) in each spot. Spatial resolution of the samples was 5 mm. The samples shown in red indicate gypsum; those in blue indicate carbonate, and those in yellow, a mixture of both minerals. Red squares indicate the place where U–Th dates were obtained (G: in gypsum, A: in aragonite).

https://doi.org/10.1016/j.yqres.2013.09.004 Published online by Cambridge University Press

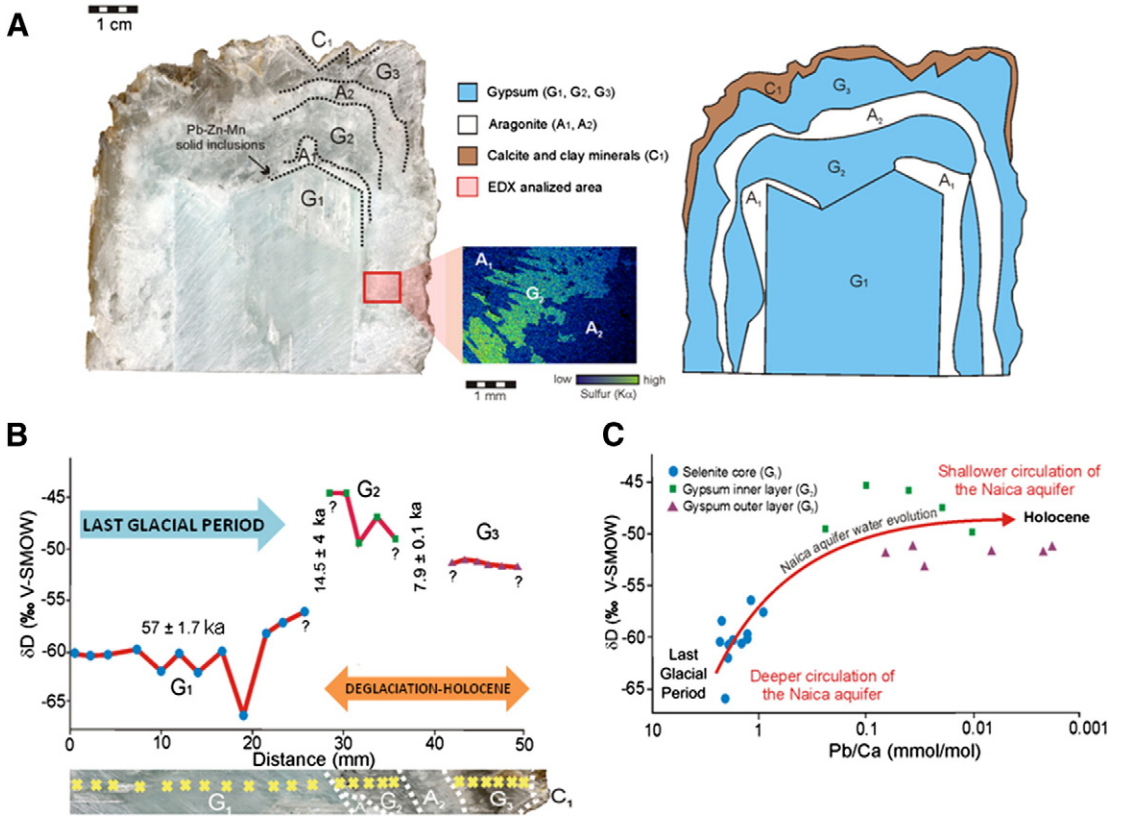

Figure 4. Mineralogical and geochemical compositions and longitudinal section of an espada speleothem. A. Photograph and micro-stratigraphical scheme showing the selenite core (G_1), two layers of microcrystalline gypsum (G_2 and G_3) and two layers of aragonite intercalations (A_1 and A_2). The outer layer is of cemented clays (C_1). Sulfur content mapping was elaborated by microprobe EDX analysis and revealed the aragonite–gypsum contact; B. Isotopic evolution (δD) of the water from which the gypsum of the espada speleothems was precipitated, obtained from the isotope composition of the hydrogen in the water of crystallization of gypsum from gypsiferous samples (extracted from a 5 cm longitudinal segment taken along the main growth axis of the speleothem). Question marks represent the growth hiatuses of unknown age (re-dissolution or no precipitation) that could have occurred between gypsum and aragonite precipitation stages; C. δD‰ (V-SMOW) and Pb/Ca ratio (mmol/mol) of the gypsiferous samples extracted from a 5 cm longitudinal segment taken from the main growth axis of the speleothem. Analytical reproducibility of Pb/Ca was ±7% and is smaller than the symbol. Note the logarithmic scale of the X axis.

previously utilized to analyze isotopes in gypsum water of crystallization (Sofer, 1978; Pradhananga and Matsuo, 1985; Hodell et al., 2012), allows for the analysis of small gypsum samples and so provides higher spatial resolution.

The internal standards used were hexatriacontane (EEZ-24; δD = −207‰), polyethylene foil (PEF; δD = −100.3‰) and coumarin (CUM; δD = 65‰). These standards were used to estimate analytical reproducibility, and their δD values are relative to the international V-SMOW (*Vienna-Standard Mean Ocean Water*) standard. Analytical reproducibility of δD was better than ±1.5‰, relative to the standard measurements. The analyses were performed in the Stable Isotope Biogeochemistry Laboratory at the CSIC Experimental Station at Zaidín (Granada, Spain).

$\delta^{18}O$ and $\delta^{13}C$ in carbonate

The carbonate bands of the speleothem were analyzed for $\delta^{13}C$ and $\delta^{18}O$. This was done by reacting 1.2 mg of sample with high-purity anhydrous H_3PO_4 at a constant temperature of 50°C for 5 h. Carbonate analysis used Gas Bench II coupled to an IRMS Delta Plus XL (Thermo Finnigan). This instrumentation allowed $\delta^{18}O$ and $\delta^{13}C$ (V-PDB) to be measured simultaneously with a reproducibility of ±0.2‰ in both cases, based on standard measurements. Values of the standards (EEZ-1, EEZ-5 and EEZ-10 — all pure carbonate and repeatedly calibrated with respect to the international standards NBS-19 and Carrara), varied from −2.57‰ to −21.57‰ for $\delta^{18}O$ and 2.59‰ to −37.21‰ for $\delta^{13}C$, compared to the international V-PDB (*Vienna-PeeDee Belemnite*) standard. The analyses were performed in the Stable Isotope Biogeochemistry Laboratory at the CSIC Experimental Station at Zaidín (Granada, Spain).

Trace-element analyses

Trace elements in powdered gypsum samples were analyzed using a Thermo iCAP DUO 6300 Inductively Coupled Plasma Atomic Emission Spectrometer installed in the Department of Geology at the University of Oviedo (Spain). The powdered samples (1 mg) were dissolved in high-purity 2% HNO_3. Major elements were measured in radial mode and trace elements in axial mode. Calibration employed international standards prepared to match typical ratios of trace and major elements in samples, and was conducted offline using the intensity ratio method described in previous work (de Villiers et al., 2002). All trace-element data are reported in mmol trace/mol Ca. Analytical errors based on repeated measurements of the standards ranged between 1% for Sr/Ca and 11% for Cu/Ca.

^{230}Th–^{234}U dating method

The age of the espada speleothems was determined using ^{230}Th–^{234}U dating. 10 g of gypsum and 0.1 g of aragonite were dissolved in 600 ml and 15 ml of ultrapure 1 M HNO_3, respectively. Actinides are selectively retained using Eichrom TRU resin, directly from solution. Further information on the analytical method for actinide separation of these samples can be found in Sanna et al. (2010).

Isotopic measurements were performed on a Nu Plasma HR multicollector ICP-MS with a U–Pb collector block at the Department of Geology, University of Oslo. Analyses were done in dry plasma using a DSN-100 desolvating nebuliser. The reproducibility of each measured $^{234}U/^{238}U$ ratio was 0.11% (2σ) (Sanna et al., 2010). Data

https://doi.org/10.1016/j.yqres.2013.09.004 Published online by Cambridge University Press

reduction, error optimization and propagation were done using tailored software (Lauritzen and Lundberg, 1997), rewritten for the Windows environment. Correction for detrital ^{230}Th contamination was needed due to the relatively low $^{230}Th/^{232}Th$ ratios found in the samples. Correction was done assuming "world mean" initial $^{230}Th/^{232}Th$ of 1.5 (Richards and Dorale, 2003). Sampling for a more complete chronology is infeasible now because of closure of the mine to visitors.

Results

Gypsum crystals cover the cave walls of the Cueva de las Espadas, and especially its lower level, from the cave floor to a height of approximately 6 m (140 to 135 m below the mine entrance). On the upper cave level (between 135 m and 120 m depth) there is evidence of gypsum crystal dissolution and carbonate wall corrosion by condensation water. Currently, dissolution of gypsum speleothems is still active, particularly close to the cave entrance. As noted above, gypsum crystals on the lower level are covered by whitish or brownish carbonate concretions, while crystals more than 2 m above the cave floor are completely clear and transparent.

Examination of a longitudinal polished section of the espada speleothem, both by mico-Raman and EDX mapping, indicated up to seven distinct phases of mineral growth (Fig. 4A). The speleothem core consists of a high-purity euhedral selenite crystal (G_1) as revealed by typical Raman signals for gypsum. The selenite crystal is overgrown by several alternating layers of carbonate and microcrystalline gypsum. First, a 1-mm-thick layer of aragonite appears around the selenite core (A_1). Subsequent alternating layers are composed of gypsum (G_2 and G_3) and aragonite (A_2), whereas the final brownish layer is made of calcite and cemented clay (C_1). The sulfur concentration in the EDX images also reveals this gypsum–carbonate alternation (Fig. 4A). In addition, solid Zn–Mn–Pb inclusions in the aragonite have been observed in the espada speleothems, at the junction between the gypsum and aragonite layers.

The $^{30}Th/^{234}U$ dating method suggests that the innermost aragonite layer (A_1) of the espada speleothems dates to 14.5 ± 4 ka, during deglaciation following the Last Glacial Maximum (<19 ka), while the outermost aragonite layer (A_2) dates to 7.9 ± 0.1 ka, during the Holocene (Table 1). The selenite crystal core (G_1) is dated to 57 ± 1.8 ka, during the last glaciation (Sanna et al., 2010). Note that these data represent the average age of a large portion of the gypsum crystals, as a consequence of the large amount of gypsum necessary for the U–Th analysis (Fig. 3) (Sanna et al., 2010).

With regard to carbonate samples, the $\delta^{13}C$ (V-PDB) ranges between −2.7 and −1.0‰, with a mean of −1.6‰ (n = 19). The $\delta^{18}O$ values of the carbonate layers range between −7.0‰ and −10.9‰, with a mean of −9.5‰ (Table 2). No correlation is observed between $\delta^{13}C$ and $\delta^{18}O$ ($R^2 = 0.1$).

Three groups of hydrogen isotopes (δD) of gypsum samples were identified (Fig. 4C and Table 3). The first corresponds to the selenite core of the espada speleothem (G_1), with a δD of −73‰ (n = 18). The second gypsum group corresponds to layer G_2 and has a mean δD of −60.1‰ (n = 5). The third group corresponds to the outmost gypsum layer of the speleothem (G_3) and has an intermediate isotope value of −64.6‰ (n = 8).

Regarding the trace elements contained in the gypsum, two different groups of samples were differentiated. The first group of samples, taken from the selenite core (G_1), is richer in trace elements (Table 3) compared to those extracted from the external gypsum layers (G_2 and G_3). The depletion ranges between 1.7% for Na/Ca and −84.7% for Cd/Ca (Fig. 8).

Table 2
Results of isotopic analysis in the carbonate samples represented in Fig. 3. Analytic reproducibility for $\delta^{13}C$ and $\delta^{18}O$ was better than ±0.2‰.

Data referred to Fig. 3A		
Samples	$\delta^{13}C$‰(V-PDB)	$\delta^{18}O$‰(V-PDB)
10B	−1.3	−7.9
11B	−1.3	−8.2
12B	−1.4	−7.0
13B	−2.6	−8.4
18	−1.7	−7.5
19	−1.1	−10.7
20	−2.0	−10.9
26	−2.0	−8.5
Data referred to Fig. 3B		
Samples	$\delta^{13}C$‰(V-PDB)	$\delta^{18}O$‰(V-PDB)
6	−1.8	−10.4
7	−1.0	−10.7
8	−1.1	−10.9
9	−1.4	−10.7
10	−1.2	−11.0
11	−1.2	−10.8
12	−1.1	−11.0
−7	–	–
−8	−2.7	−8.6
−9	−1.3	−8.6
−10	−1.1	−9.4
−11	−2.0	−9.2

Discussion

Mineralogy and genesis of the espada speleothems

The precipitation of selenite speleothems in the hypogenic caves of Naica is a consequence of the upward flow of thermal water in the system (García-Ruiz et al., 2007). During the first hypogenic stages, oxidation of metal sulfides enriched the groundwater in sulfates, resulting in precipitation of anhydrite at high temperature. In later phases, anhydrite started to dissolve as the aquifer temperature gradually fell to around 58°C, as revealed by fluid inclusion analyses (Garofalo et al., 2010). At this temperature, the solubility of anhydrite and gypsum is the same, whereas at lower temperatures, gypsum is the predominant mineral phase (Hardie, 1967) and it precipitates as selenite crystals.

The exceptional size of the speleothems in the Naica mine is a consequence of the extremely slow nucleation and growth rate that result from the constant low level of saturation over a long period (García-Ruiz et al., 2007). In fact, the selenite crystals of the Naica caves have been recently identified as having the slowest growth rate thus far described in nature ($1.4 \pm 0.2 \times 10^{-5}$ nm/s, Van Driessche et al., 2011).

The espada speleothems of Cueva de las Espadas comprise a high-purity selenite core overlain by successive deposits of calcite, gypsum and aragonite. Whereas the precipitation of the selenite crystals in this cave was similar to the generation of the huge selenite crystals in the deeper Cueva de los Cristales (García-Ruiz et al., 2007; Forti, 2010)

Table 1
Uranium concentration, measured U and Th activity ratios and ages of subsamples from the espada speleothems of Cueva de las Espadas.

Samples	Mineral	U (ppm)	$^{234}U/^{238}U$	$^{230}Th/^{234}U$	$^{230}Th/^{232}Th$	Age, ka	2σ+ ka	2σ− ka	Corr. age	2σ+ ka	2σ− ka
G_1	Gypsum	0.046	2.36105 ± 0.0109	0.44666 ± 0.0773	19 ± 18.62	60.46	0.07	0.07	57.010	1.77	1.77
A_1	Aragonite	0.163	2.97474 ± 0.0294	0.13186 ± 0.0334	29 ± 7.43	15.21	4.14	4.02	14.491	4.15	4.03
A_2	Aragonite	0.200	3.42787 ± 0.00671	0.070327 ± 0.000846	949 ± 20	7.87	0.04	0.04	7.863	0.04	0.04

https://doi.org/10.1016/j.yqres.2013.09.004 Published online by Cambridge University Press

Table 3
δD in gypsum water of crystallization and trace-element composition (Tr/Ca in mmol/mol) of the gypsum samples. The δD of the original water from which gypsum was derived have been also calculated. Nomenclature of the samples refers to Fig. 3. Analytical reproducibility of δD was better than ± 1.5‰.

Samples	Gypsum layer	δD‰ (V-SMOW) gypsum crystallization water	δD‰ (V-SMOW) mineral-forming water	As/Ca	Cd/Ca	Pb/Ca	Zn/Ca	Cr/Ca	Cu/Ca	Fe/Ca	Ni/Ca	K/Ca	Mg/Ca	Sr/Ca	Na/Ca
15B	G_3	−65.9	−51.6	0.125	0.105	0.655	28.16	0.007	1.336	0.010	0.005	0.135	8.797	4.935	0.306
14B	G_3	−65.8	−51.5	0.099	0.010	0.022	1.106	0.012	0.222	0.018	0.001	0.108	1.841	0.936	0.117
7B	G_1	−66.8	−52.5	0.731	2.302	1.363	23.489	0.003	3.143	0.006	0.005	0.190	21.841	9.961	0.530
6B	G_1	−66.4	−52.2	0.699	2.668	1.633	9.263	0.002	0.602	0.008	0.000	0.103	9.493	1.464	0.299
5B	G_1	−67.3	−53.1	0.198	0.421	0.165	3.479	0.005	0.187	0.010	0.002	0.078	3.145	1.035	0.115
4B	G_1	−76.7	−62.6	0.443	2.121	0.901	5.812	0.004	0.334	0.004	0.017	0.101	6.119	1.052	0.302
3B	G_1	−79.3	−65.3	0.383	1.884	1.137	8.026	0.022	1.320	0.390	0.050	0.647	6.698	1.413	0.502
2B	G_1	−78.1	−64.1	0.533	2.085	1.239	10.532	0.004	0.903	0.015	0.002	0.129	9.248	7.180	0.281
1B	G_1	−64.1	−49.8	0.270	0.935	0.660	5.979	0.019	0.776	0.028	–	0.129	6.833	3.812	0.309
0	G_1	−72.9	−58.8	0.924	3.426	1.803	12.586	0.003	0.856	0.096	0.004	0.171	17.839	2.456	0.519
1	G_1	−73.2	−59.0	0.368	1.502	1.482	6.155	0.002	0.686	0.010	0.002	0.151	6.625	4.239	0.258
2	G_1	−73.1	−59.0	0.617	2.335	1.784	8.030	0.012	0.529	0.031	0.003	0.178	10.446	6.347	0.342
3	G_1	–	–	0.574	2.497	1.293	9.516	0.219	0.929	1.047	0.038	0.139	10.047	2.331	0.333
4	G_1	−72.4	−58.3	–	–	–	–	–	–	–	–	–	–	–	–
5	G_1	−74.7	−60.6	1.293	4.724	1.938	17.734	0.007	1.079	0.041	0.003	0.222	17.449	1.535	0.541
6	G_1	−73.0	−58.8	0.873	3.322	1.728	18.636	0.003	2.229	0.021	0.009	0.257	19.472	5.039	0.644
7	G_1	−74.8	−60.7	0.784	2.763	1.920	20.815	0.003	2.999	0.009	0.009	0.231	23.291	2.631	0.626
8	G_1	−72.8	−58.7	0.723	2.907	2.344	13.846	0.005	1.454	0.013	0.003	0.207	15.502	4.112	0.439
9	G_1	−78.8	−64.8	0.190	0.824	2.027	3.185	0.003	0.273	0.008	–	0.101	4.844	4.052	0.260
10	G_1	−71.0	−56.8	0.189	0.774	2.273	4.083	0.000	0.443	0.058	0.002	0.095	5.017	4.644	0.171
11	G_1	−70.1	−55.9	0.361	1.297	0.906	10.025	0.002	1.243	0.029	0.006	0.119	10.602	4.891	0.297
12	G_1	−69.1	−54.9	0.299	1.123	1.158	8.737	0.002	1.305	0.111	0.004	0.117	19.893	2.281	0.386
13	G_2	−57.8	−43.5	–	0.030	0.029	0.667	0.005	0.136	0.013	0.000	0.139	5.203	0.936	0.644
14	G_2	−57.9	−43.5	0.040	0.006	0.014	0.590	0.007	0.136	0.015	0.002	0.121	2.244	2.215	0.217
15	G_2	−62.4	−48.1	0.031	0.009	0.011	0.753	0.005	0.139	0.010	0.002	0.107	3.842	2.221	0.282
16	G_2	−60.1	−45.8	0.057	0.005	0.020	0.825	0.003	0.158	0.020	0.000	0.116	2.936	0.600	0.177
17	G_2	−62.2	−47.9	0.041	0.048	0.249	2.306	0.005	0.349	0.004	0.002	0.089	5.776	1.946	0.167
20	G_3	−65.2	−51.0	–	–	–	–	–	–	–	–	–	–	–	–
21	G_3	−63.6	−49.3	0.046	0.003	0.038	0.238	0.010	0.080	0.041	–	0.153	0.535	0.914	0.109
22	G_3	−63.8	−49.5	0.037	0.000	0.002	0.161	0.000	0.036	0.009	0.001	0.108	0.375	0.679	0.101
23	G_3	−64.1	−49.8	0.046	0.002	0.007	0.222	0.003	0.086	0.020	–	0.150	0.541	0.632	0.422
24	G_3	−64.2	−49.9	0.037	0.001	0.003	0.205	0.000	0.053	0.007	0.000	0.112	0.664	0.538	0.164
25	G_3	−64.3	−50.0	0.129	0.067	0.067	3.902	0.006	0.516	0.025	0.002	0.152	7.293	1.516	0.216

(Figs. 5A and 6A), the outer alternating gypsum and carbonate layers require a more complex explanation.

These thin mineral layers coat the selenite crystals that were precipitated during previous stages, but they only appear over speleothems that lie close (<2 m) to the floor of the cave. This fact suggests that, during certain phases, the water table of the Naica aquifer fell beneath the cave level and a cave pool formed at the cave bottom, whose surface lay around 2 m from the cave floor in the lower level of the Cueva de las Espadas. Thus, vadose conditions intervened in the upper part of the caves, interrupting the subaqueous precipitation of gypsum, while mineral precipitation (in this case, carbonate), occurred in the lake at the bottom of the cave (Figs. 5B, 6C).

When vadose and oxic conditions prevailed in the upper part of the cave, the precipitation of polymetallic oxyhydroxides also took place in the lake; in the espada speleothems, this process is revealed by the presence of polymetallic inclusions in the aragonite layers (Figs. 4A and 6B) (Gázquez et al., 2012).

During the vadose stage, the upper part of the cave, further from the thermal water, started cooling more rapidly, while the lake maintained a slightly higher temperature due to greater proximity to the main phreatic level. As a consequence, considerable evaporation from the lake surface took place and condensation occurred on the cooler cave roof and walls (Fig. 5B). The cavity was practically sealed and so condensation water, laden with CO_2, was returned to the cave lake. Gypsum crystals present in the upper levels of the cave dissolved, supersaturating the water lake in calcium carbonate.

Accordingly, it can be deduced that at 14.5 ± 4 ka, and later at 7.9 ± 0.1 ka, – corresponding to the intervals when the aragonite layers were precipitated (Sanna et al., 2010, 2011) – the bottom of the Cueva de las Espadas became a perched underground lake. The lake formed as a consequence of the falling water table (Figs. 5B and 6C) and was unconnected to the thermal aquifer. The temperature at which aragonite precipitation occurred in the Cueva de las Espadas, which was lower than the temperature for gypsum generation (as we describe below), also supports this assertion.

During this period, due to the partial disconnection of the main phreatic level, no CO_2 would be carried into the lake by the aquifer water. The only possible source of additional CO_2 was the cave atmosphere, where a continuous CO_2 supply was assured from the vapors rising through the conduits linking the cave to deep thermal reservoirs (Gázquez et al., 2012). Deposition of calcium carbonate was induced by direct diffusion of carbon dioxide present in the cave atmosphere into the lake water or, more probably, by solution of CO_2 in the cave atmosphere into the condensing water that later dripped into the lake. Under these circumstances of high Ca^{2+} concentration in lake water and an alkaline environment (given that the cave developed in a marine carbonate deposit), aragonite could easily precipitate, conditioned only by the pH of the solution. Although the CO_2 input into the Cueva de las Espadas lake would have caused slight acidification of the water, this could have been buffered by the dolomite host rock which also supplied Ca^{2+} and Mg^{2+} to the solution. Precipitation of aragonite is typical of solutions with a high Mg/Ca ratio, because the Mg^{2+} ion inhibits crystallization of calcite and favors precipitation of its polymorph (Burton and Walter, 1987).

This mechanism of carbonate precipitation arising from diffusion of CO_2 in saturated gypsum-rich waters has been reported previously in gypsiferous environments (Forti, 2003) and also in a carbonate environment (Onac and Forti, 2011). This mechanism was proved to be currently active at the −590 m level in the Naica mine (Forti et al., 2008), and was the cause of aragonite and calcite precipitation in the Ojo de la Reina Cave (Badino et al., 2011) at the −290 m level.

Subsequently, the water table rose resulting in further phreatic conditions: the cave was totally underwater and so gypsum started precipitating again, though in a different framework. The degree of saturation

https://doi.org/10.1016/j.yqres.2013.09.004 Published online by Cambridge University Press

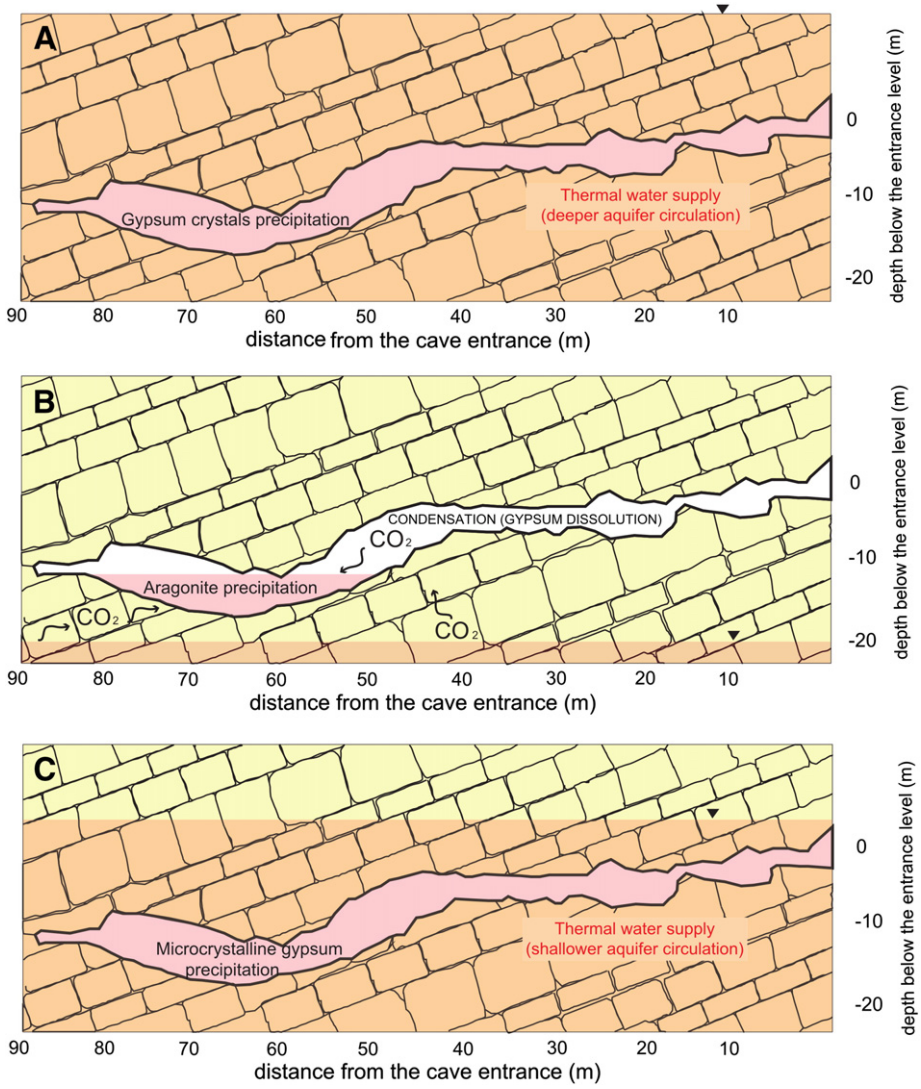

Figure 5. Evolutionary diagram of the water table position in the Cueva de las Espadas. Note that distances are referred to the cave entrance level (0, 0). A. Precipitation of gypsum crystals when the cave was totally under water conditions and deeper circulation of the Naica aquifer; B. Precipitation of aragonite in a pool that occupied the cave bottom as a result of the drop of the water table. The upper part of the caves was under vadose conditions and condensation on the cave walls took place, giving rise to dissolution of gypsum precipitated during previous stages and carbonate host rock corrosion; C. Precipitation of microcrystalline gypsum under phreatic conditions and shallower circulation of the Naica aquifer. Less stable conditions took place than during the previous stages of selenite crystal precipitation (topography provided by La Venta Exploring Team).

of the lake water with respect to gypsum was higher than during the previous selenite precipitation stage, and so precipitation of microcrystalline gypsum occurred (Figs. 5C and 6D). During the previous vadose stage, gypsum crystals on the roof and walls in the upper part of the cave would have been exposed to the cave atmosphere. The condensation water would have enhanced the dissolution of these older gypsum crystals so that the subsequent phase of microcrystalline gypsum precipitation (G_2) was much faster. In fact, partial dissolution of gypsum crystals by condensation water was shown to open large fluid inclusions inside selenite crystals in other cavities of the Naica Mine, such as Ojo de la Reina Cave, which produced high to extremely high saline content in the drip water (Badino et al., 2011).

Speleological evidence, such as the corroded and dissolved selenite crystals in the upper part of the cave (Forti and Sanna, 2010) also suggests that this part of the cavity was included in the vadose zone above the water table during some periods.

Another source of calcium sulfate was the widespread presence of anhydrite in the host rock, which provided an additional supply of calcium sulfate into solution (García-Ruiz et al., 2007). As a result, when phreatic conditions were restored due to the water table rising, gypsum saturation was high enough for gypsum deposition to restart immediately in Cueva de las Espadas, while aragonite precipitation ceased (Fig. 5C).

The fluid inclusions in the gypsum layer that were precipitated during this stage (G_2) had a relatively high salinity (7.7 eq. wt% NaCl), higher than the salinity analyzed in the gypsum core (G_1) (5.3 eq. wt% NaCl) (Garofalo et al., 2010). This provides clear evidence that the above-mentioned key mechanism (which led to higher gypsum saturation in the solution than during previous stages) is correct and was responsible for the precipitation of microcrystalline gypsum in Cueva de las Espadas (Fig. 5C).

After this stage, a further lowering of the water table led again to vadose conditions in the upper part of the cave, while a cave pool occupied the lower part of the cavity. In this situation, gypsum precipitation ceased and aragonite (A_2) precipitation began again, caused by CO_2 diffusion from the cave atmosphere into the lake water (Fig. 6E). Later, the water table rose again and allowed precipitation of a new gypsum layer (G_3) (Fig. 6F). Subsequently, once the water table dropped permanently below the cave level, a thin calcite layer was precipitated (C_1), probably under cooler conditions after 1950 due to the mine dewatering for the

https://doi.org/10.1016/j.yqres.2013.09.004 Published online by Cambridge University Press

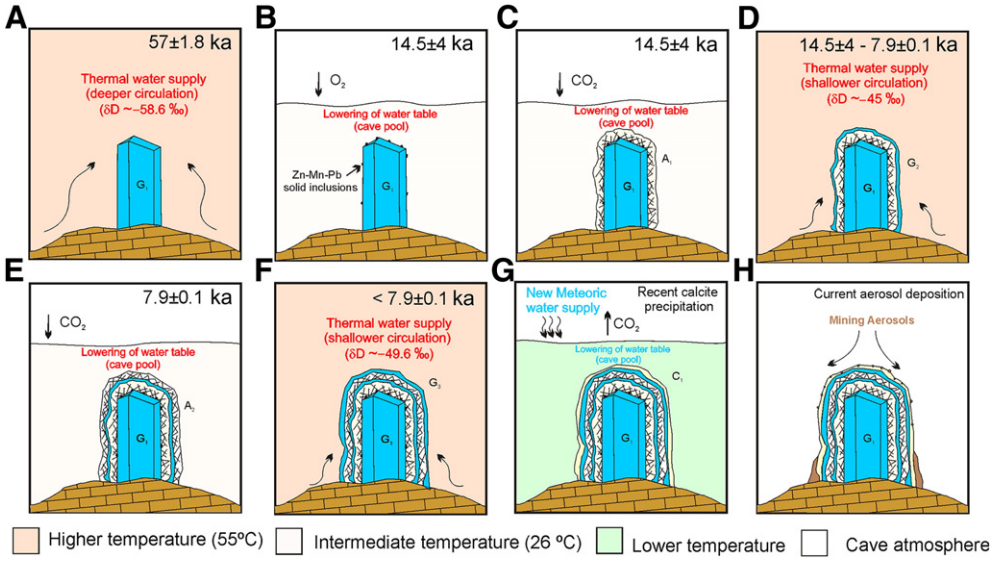

Figure 6. Evolutionary diagram of an espada speleothem in the Cueva de las Espadas. A. Precipitation of the selenite core (G_1) under phreatic conditions and deeper circulation of the aquifer during the last glaciation (ca. 57 ka) (Fig. 5A); B. Precipitation of Zn–Mn–Pb solid inclusions under oxygenic conditions; C. Precipitation of the first layer of aragonite (A_1) in a pool at the cave bottom at intermediate temperature. At this time, vadose conditions prevailed in the upper part of the cave due to the falling water table during a brief period of the deglaciation (Fig. 5B); D. Precipitation of microcrystalline gypsum (G_2) when the cave was totally under phreatic conditions and shallower circulation of the Naica aquifer during periods of the deglaciation and the early Holocene (Fig. 5C); E. Precipitation of a second aragonite layer (A_2) under lowest recharge conditions at intermediate temperature during the early Holocene; F. Precipitation of a second microcrystalline gypsum layer (G_3) under phreatic conditions during the Holocene; G. Precipitation of calcite (C_1) under vadose conditions with falling temperature; H. Mining aerosols and cemented clay deposition under atmospheric cave conditions in a recent period.

mining activities (Fig. 6G). Finally, when the cave was intercepted by the mine galleries, mining activity generated particles in suspension that were deposited over the espada speleothems of Cueva de las Espadas (Fig. 6H).

Paleohydrogeochemical evolution of the Naica aquifer

δD of gypsum water of crystallization is around 19‰ lower than the solution water from which it derives (Fontes and Gonfiantini, 1967; Pradhananga and Matsuo, 1985). Isotope fractionation of hydrogen isotopes ($\alpha D_{gyp-H_2O} = 0.985$) is virtually independent of temperature below 58°C (Fontes and Gonfiantini, 1967; Hodell et al., 2012). By using this fractionation factor we calculated that the δD of the aquifer water (which we assume to be equal to the solution from which gypsum precipitated in Cueva de las Espadas) ranged between −43.5 and −65.3‰ (Fig. 4B) from the δD of gypsum (Table 3). These values are typical of meteoric water in the Naica setting (Cortés et al., 1997) and suggest that the saline solution that generated the espada speleothems consisted of meteoric water, which infiltrated into the Naica aquifer and underwent changes in chemical composition and temperature.

The δD value of the current Naica groundwater (δD = −57.5 ± 0.7‰: García-Ruiz et al., 2007) is within the range obtained in our study (−65.3 to −43.5‰). On the other hand, the estimated $\delta^{18}O$ values from the LMWL in Chihuahua ($\delta D = 7\ \delta^{18}O + 1.9$ by Cortés et al., 1997) using δD data inferred from gypsum are between −9.6‰ and −6.8‰. These values match with those reported by García-Ruiz et al. (2007) ($\delta^{18}O = -7.65 \pm 0.15$‰) for current aquifer water.

In particular, the isotopic composition (δD) of the Naica aquifer at around 57 ka (from G_1) was around −58.6‰, while the value for $\delta^{18}O$ was −8.6‰, estimated from the LMWL in this area. Meanwhile, the inferred mean values of δD and $\delta^{18}O$ of the aquifer during the deglaciation and the Holocene (gypsum precipitated from 14.5 ± 4 to 7.9 ± 0.1 ka and after 7.9 ± 0.1 ka, from G_2 and G_3) was around −48.6‰ and −7.2‰, respectively (Figs. 4B and C).

The $\delta^{18}O$ and $\delta^{13}C$ values in carbonate speleothems usually record the $\delta^{18}O$ water and the $\delta^{13}C$ of dissolved inorganic carbon species, respectively (Fairchild et al., 2006). In particular, the $\delta^{13}C$ value of precipitated carbonate in caves usually depends on the source of CO_2 as well as the intensity of the CO_2 degassing into the cave atmosphere. The $\delta^{13}C$ values (−1.59‰ on average) found in the espada speleothem are higher than the typical values of carbonate speleothems in other caves (Fairchild et al., 2006) where soil and vegetation are the main CO_2 sources. The extremely weak correlation between $\delta^{13}C$ and $\delta^{18}O$ in the carbonate of the espada speleothem ($R^2 = 0.1$) indicates that intense CO_2 degassing and a high evaporation rate were not principal players in the precipitation of the aragonite. This is in contrast to the mechanism of isotopic enrichment in speleothems observed in other caves (Baker et al., 1997). It suggests that, in the hypogenic aquifer of Naica, the main carbon source is the CO_2 derived from dissolution of the marine limestone host rock. ^{13}C contribution from host rock has been also proposed as the cause of high $\delta^{13}C$ values in speleothems from other caves (Spötl and Mangini, 2007).

In regard to oxygen isotopes in the carbonate, Patterson et al. (1993) calculated the $\delta^{18}O$ fractionation during aragonite precipitation from dissolved inorganic carbon in water:

$$\Delta\delta^{18}O_{A-W} = 18.56(\pm 0.319) \cdot 10^3 \times T^{-1} - 33.49(\pm 0.307)$$

where $\Delta\delta^{18}O_{A-W}$ is the isotopic fractionation between aragonite and inorganic carbonate species dissolved in water during precipitation (V-SMOW), and T (K) is the water temperature at equilibrium.

Applying this equation to the $\delta^{18}O$ data for the aragonite layers of the espada speleothem (≈−7 to −10‰ V-PDB) (Table 2) suggests that the values of $\delta^{18}O$ in the aquifer water were similar to those expected for carbonate precipitation from meteoric water in this area (≈−7 to −8 V-SMOW: Cortés et al., 1997), and also similar to the present-day aquifer water (−7.6 ± 0.1‰ V-SMOW: García-Ruiz et al., 2007). It is considered that the aragonite precipitation occurred in a perched lake unconnected to the aquifer when the water table was beneath the Cueva de las Espadas, so the water temperature had to be lower than during gypsum precipitation (<58°C). Isotopic equilibrium has been also assumed. In contrast, the influence of juvenile water during the genesis of the espada speleothems must have been minimal, since magmatic water could have low δD values but not low $\delta^{18}O$ values (Hoefs, 2004).

https://doi.org/10.1016/j.yqres.2013.09.004 Published online by Cambridge University Press

On the other hand, once the isotopic composition of the Naica aquifer from 14.5 ± 4 to 7.9 ± 0.1 ka and after 7.9 ± 0.1 ka is inferred for gypsum water of crystallization, these $\delta^{18}O$ values can be used to estimate the approximate temperature at which carbonate precipitated in the perched lake of Cueva de las Espadas during deglaciation and the Holocene, by applying the equation obtained by Patterson et al. (1993) for isotopic fractionation during aragonite precipitation.

The mean $\delta^{18}O$ value of aragonite (−9.5 ± 1.4‰ V-PDB) was used to calculate the aquifer water temperature during the precipitation under two different scenarios for $\delta^{18}O$: (1) in the aquifer water estimated from gypsum water of crystallization younger than 14.5 ± 4 ka (G_2 and G_3) (−7.2 ± 0.4‰ V-SMOW) and (2) in the current aquifer water (−7.6 ± 0.1‰ V-SMOW; García-Ruiz et al., 2007). Since the $\delta^{18}O$ values observed in the paleogroundwater (estimated from gypsum layers G_2 and G_3) are so similar to those in the current aquifer water, we assume that the $\delta^{18}O$ of the solution from which aragonite precipitation occurred was not very different from these isotopic values.

The lake water temperature obtained for 14.5 ± 4 ka and 7.9 ± 0.1 ka in Cueva de las Espadas, based on $\delta^{18}O$ of gypsum water of crystallization was 27.8 ± 6.2°C, whereas calculations based on $\delta^{18}O$ of the current aquifer gave a temperature of around 25.7 ± 5.9°C (Fig. 7). In both cases, the deduced water temperature was considerably lower than during the phase of selenite crystal precipitation (estimated from fluid inclusion analyses to be ≈58°C; Garofalo et al., 2010), and lower than the current aquifer temperature (52–54°C; Forti, 2010). Consequently, it can be asserted that the isotopic composition of the Naica aquifer ($\delta^{18}O$) has not changed much from 14.5 ± 4 ka to the present, as revealed by the similar values of $\delta^{18}O$ inferred from gypsum water of crystallization and the current aquifer (−7.2 ± 0.4‰ and −7.6 ± 0.1‰, respectively). Similarly, the water temperature of the Naica aquifer has not practically changed from 14.5 ± 4 ka to the present, remaining at around 52–58°C. Nevertheless, the water temperature at the Cueva de las Espadas level changed from 58°C, when gypsum precipitated, to ≈27°C, when the aragonite precipitation occurred.

These data strongly support the assertion that the Cueva de la Espadas lake was perched above the water table and unconnected to the deep thermal circulation of the Naica aquifer during the phases of carbonate precipitation around 14.5 ± 4 ka and 7.9 ± 0.1 ka.

At the same time, the δD of gypsum water of crystallization and the trace elements coprecipitated in gypsum have been useful indicators of different hydrogeological regimes that occurred in the Naica aquifer over the period of formation of the espada speleothems. The negative covariation of δD composition and Pb/Ca ratios in gypsum during the formation of successive stages of these speleothems (Fig. 4C) suggests changes in the source of meteoric water (Pacific Ocean/Gulf of Mexico), which were coupled to changes in groundwater circulation in the Naica aquifer (deeper/shallower aquifer circulation).

Water–rock interaction under thermohaline conditions extracts higher concentrations of heavy and transition metals due to the highly stable Cl^- and SO_4^{2-} complexes (Irving and William, 1953; Gardner and Nancollas, 1970; Sherman, 2010). Accordingly, the Pb/Ca ratio in the gypsum of the espada speleothems might have been higher when precipitation occurred from deeper thermal water in at the Naica aquifer over the last glaciation, in particular around 57 ka. During this period, groundwater circulation was greater due to the increased recharge into the aquifer; thus, metal extraction from the ore bodies in the host rock was enhanced, as revealed by the higher trace-element content in the gypsum core of the espada speleothem ca. 57 ka. In contrast, gypsum deposited during later stages (after 14.5 ± 4 ka) was derived from shallower water that was depleted in dissolved metals as a consequence of the lower recharge and more limited groundwater circulation during some periods of the deglaciation and the Holocene (Fig. 4C).

Like Pb, a broad array of heavy and transition metals reveal strong enrichment in the selenite core compared to the subsequent gypsum layer, confirming the greater influence of the circulation from the deeper aquifer in the earliest phase of the espada speleothem growth (Fig. 8).

The depletion in trace elements of the first gypsum layer (G_2) compared to the gypsum core (G_1) varied between 1.7% for Na and −84.7% for Cd (Fig. 8). Earlier work by Lu et al. (1997) demonstrated that the presence of fluid inclusions might affect the determination of trace elements in gypsum, in particular Na and Mg whose concentrations in fluid inclusion are usually high. In contrast, these authors found that other elements, present in low concentration in fluid inclusions, are unaffected by the proportion of fluid inclusions in gypsum. Thus, enrichment in heavy and transition metals (Pb, Cd, As, Fe, Zn) compared to lighter metals (K, Sr) reflects the greater complexation affinity of the heavy and transition metals with Cl^- and SO_4^-, which significantly increases their solubility in saline thermal waters (Irving and William, 1953). This mechanism of metal mobilization was more effective under the more abundant and deeper circulation of the Naica aquifer that occurred ca. 57 ka during the last glaciation than during the periods from 14.5 ± 4 to 7.9 ± 0.1 ka and after 7.9 ± 0.1 ka, recorded by the espada speleothems, when water circulation was less.

Paleoenvironmental record of the espada speleothems

On the basis of the age of the central gypsum core of the speleothems (G_1) we suggest that higher recharge occurred in the Naica aquifer ca.

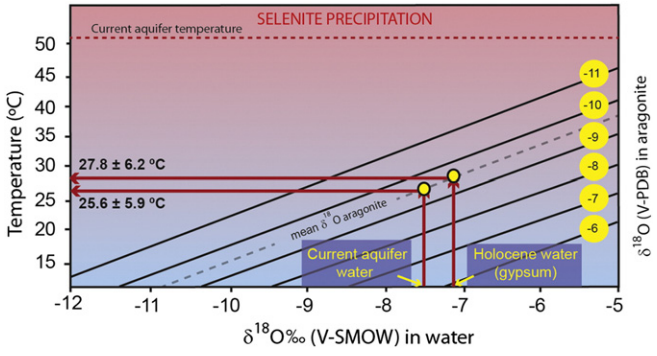

Figure 7. Estimated water temperature during aragonite precipitation obtained from the mean $\delta^{18}O$ value of aragonite (V-PDB) and the mean $\delta^{18}O$ of the aquifer water (V-SMOW) in two different frameworks: (1) inferred mean $\delta^{18}O$ value from water of crystallization of gypsum precipitated during the deglaciation and the Holocene (after 14.5 ± 4 ka; G_2 and G_3) and (2) the current mean $\delta^{18}O$ value of the groundwater in the Naica Mine (García-Ruiz et al., 2007). The geothermometric equation obtained by Patterson et al. (1993) has been used. The STD of the estimated water temperature was calculated on the basis of the STD of $\delta^{18}O$ in carbonate obtained from the espada speleothem (± 1.4‰), as well as the STD of the current water of the Naica aquifer (±0.15‰, García-Ruiz et al., 2007) and the STD of the estimated water of the Holocene (±0.4‰).

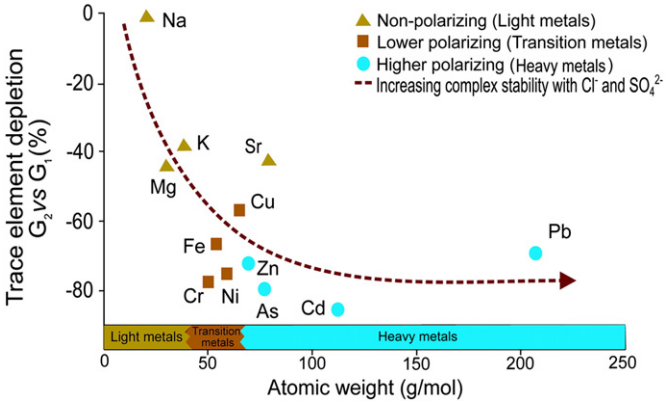

Figure 8. Depletion (%) of several trace elements $(((T_r/Ca_{gyp\ core} - T_r/Ca_{inner\ gyp\ layer}) / Tr/Ca_{gyp\ core}) \times 100)$ for G_2 compared to G_1. This factor was calculated for the mean of the ratio Tr/Ca for each element in samples of the selenite core (G_1) and the inner gypsum layer (G_2). They are represented as a function of the atomic weight of each trace element.

https://doi.org/10.1016/j.yqres.2013.09.004 Published online by Cambridge University Press

57 ka, during the last glaciation, revealing a wetter climate. During this period, the water table lay below the −90 m (the level of Cueva de los Palacios, where no traces of euhedral gypsum crystals have been found and where only gypsum speleothems formed under vadose conditions have been described), and above the −120 m depth, where the Cueva de las Espadas is located. The selenite core of the espada speleothems was laid down from a δD-depleted solution (−58.6‰ on average), when the cave level was affected by the deep circulation of the Naica aquifer during the last glaciation.

The deglaciation–early Holocene was a period of intermediate to low aquifer recharge in which carbonate (Fig. 5B) and microcrystalline gypsum (Fig. 5C) precipitated on the earlier gypsum crystals formed in Cueva de las Espadas. The water table fell and, during some intervals, it lay even below the level of the cave. Thus, a perched lake occupied the lower part of the cavity, while vadose conditions predominated in the upper levels. The periods of least recharge to the aquifer responded to brief drier intervals during the deglaciation–early Holocene, corresponding with the precipitation of the carbonate layers of the espada speleothems (Figs. 5B and 6C,E).

During the deglaciation–early Holocene, summer monsoon precipitation is documented to have been significantly reduced on several occasions by cold North Atlantic sea surface temperatures, such as during the 8.2 ka event and the Bølling/Allerød transition (Lachniet et al., 2004; Kageyama et al., 2005; Rohling and Pällke, 2005). Such intervals were characterized by a significantly reduced thermohaline circulation in the North Atlantic Ocean and were potentially dry periods in the North Atlantic region. In fact, relative dry conditions were recorded by speleothems in the Guadalupe Mountains caves (New Mexico, USA), beginning just before 14.5 ka and lasting at least until 12.9 ka, that Polyak et al. (2012) assigned to the Northern Hemisphere Bølling–Allerød oscillation, as also preserved in Greenland ice cores and other paleoclimatic proxies (Shakun and Carlson, 2010). In particular, the B/A transition was characterized by dry and warmer climate in the North Atlantic area (Monnin et al., 2001). Such circumstances could have resulted in a decrease in precipitation in northern Mexico and higher evaporation rate, leading to lower effective recharge to the aquifers. Similarly, widespread dry conditions seem to have taken place at 8.2 ka in the North Atlantic area (Alley et al., 1997), and very probably in northern Mexico.

These dry events (or others with similar characteristics regarding the age uncertainties of the aragonite layer A_1) could have led to a falling water table around 14.5 ± 4 ka and 7.9 ± 0.1 ka in the Naica aquifer as a result of lower effective recharge to the aquifer during these periods. This would have resulted in the vadose conditions in the upper part of the Cueva de las Espadas, while a perched lake occupied the lower part of the cave where aragonite could be precipitated forming the aragonite layers of the espada speleothems.

When the water table rose and submerged the cave completely, gypsum precipitation resumed (14.5 to 7.9 ka and after 7.9 ka); the gypsum layers (G_2 and G_3) of the espada speleothems were laid down but, in this case, the gypsum water of crystallization was enriched in deuterium (−45.7‰ and −49.9‰ on average). The cave was influenced by the shallower aquifer circulation, as a result of lower effective recharge of the aquifer in a drier and probably warmer climate that occurred during these intervals than during the last glaciation.

Broadly speaking, the initial gypsum growth stage of the espada speleothems indicate rising thermal water coinciding with a relatively humid period in northern Mexico, particularly around 57 ka, as revealed by the maximum speleothem growth rate recorded in other caves in nearby Texas (Musgrove et al., 2001) and New Mexico (Brook et al., 2006). Recent studies on lacustrine sediments of the Babicora paleolake (also in the Chihuahua State) indicate that this part of northern Mexico received higher-than-average precipitation at *ca.* 79–58 ka (Metcalfe et al., 2002; Roy et al., in press). In a study of lacustrine ostraecods, Chávez-Lara et al. (2012) also determined that a wetter climate prevailed at *ca.* 57 ka in the Chihuahua Desert, corroborating the assertion that there was greater recharge to the Naica aquifer during this period of the last glaciation.

The isotope record of the espada speleothems shows that, during 14.5–7.9 ka and after 7.9 ka, when gypsum precipitated, the aquifer water was enriched in deuterium by 12.8–8.7‰ relative to ca. 57 ka. This isotopic shift in the Naica groundwater was in response to variations in the moisture source of the precipitation (Pacific Ocean/Gulf of Mexico), which have been demonstrated to affect the isotopic composition of rainfall in northern Mexico. The $\delta^{18}O$ and δD values of modern summer monsoon precipitation in the Gulf of Mexico are higher than in the winter Pacific precipitation (Hoy and Gross, 1982; Yapp, 1985; Higgins et al., 1997; Asmerom et al., 2010).

In this area, recharge responds most strongly to changing precipitation delivery from the North American summer monsoon. Currently, the region receives precipitation from Pacific winter cyclones, but the majority (>70%) comes from the summer monsoon system in the Gulf of Mexico (Hoy and Gross, 1982; Yapp, 1985; Douglas et al., 1993).

Thus, the observed shift towards higher δD values in the Holocene portion of our espada speleothem sample is consistent with the greater importance of the summer monsoon precipitation, strongly indicating warmer and probably drier conditions compared to the last glaciation.

Such circumstances played a key role in determining the effective moisture in this part of North America. Probably, lower temperatures during the last glaciation resulted in a lower evaporation rate and, even if annual precipitation was the same for the deglaciation and the Holocene, a greater effective precipitation prevailed during the last glaciation (ca. 57 ka), as also revealed by paleohydrological studies in lakes of central New Mexico (Allen and Anderson, 2000).

Conclusions

The complex gypsum–carbonate espada speleothems from Cueva de las Espadas at Naica are a compelling new paleoenvironmental proxy which, by offering information on relative water table position, moisture sources and circulation regime of the aquifer, complement existing paleoclimate records from carbonate speleothems. Alternations of gypsum and carbonate layers in the espada speleothems are linked to water table oscillation in the Naica aquifer over the late Quaternary. Meanwhile, differences observed in trace-element content in gypsum precipitated ca. 57 ka and <20 ka reveal that groundwater circulation in the aquifer was more active during the last glaciation (ca. 57 ka) than during deglaciation or the Holocene (14.5 ± 4 to 7.9 ± 0.1 ka and after 7.9 ± 0.1 ka), due to the wetter climate and greater aquifer recharge during the last glaciation. In addition, the stable isotopic composition of deuterium in the gypsum provides information about the moisture source of past precipitation, without the temperature effects on isotopic partitioning that occur with oxygen isotopes in carbonate speleothems.

It is concluded that the record from the espada speleothem differentiates between a relatively humid glacial period and a drier deglaciation–Holocene. By early deglaciation time, the summer monsoon was the dominant source of precipitation; this appears to have increased vulnerability to drought, since the only exceptional – and probably brief – arid intervals occurred during deglaciation (14.5 ± 4 ka) and the early Holocene (7.9 ± 0.1 ka), probably related to the Bølling/Allerød transition and the 8.2 ka event. In consequence, aquifer recharge fell, as did the water table. The upper levels of the Cueva de las Espadas were left under vadose conditions, while the cave bottom was occupied by a lagoon where precipitation of carbonate could occur.

On the basis of these results, it can be hypothesized that the isotopic composition of other phreatic gypsum speleothems over the world – such as those from the Giant Pulpí Geode (Spain) (García-Guinea et al., 2002), the El Teniente Mine (Chile) (Klemm et al., 2007) or the Cupp-Coutunn Cave (Turkmenistan) (Maltsev, 1997; Bottrell et al., 2001) – might be used to reconstruct the geochemistry of paleogroundwater. Gypsum speleothems in caves like those of Naica occur only very rarely worldwide. These places must be conserved due to their natural

https://doi.org/10.1016/j.yqres.2013.09.004 Published online by Cambridge University Press

environmental value, and also due to their potential use in future paleoclimatic research.

Acknowledgments

Financial support was from the "PALAEOGYP" International Collaboration Project (CGL2006-01707/BTE Ministry of Science and Innovation, Spain and FEDER funds of EU), Spanish Science grant AP-2007-02799, the Water Resources and Environmental Geology Research Group (University of Almería) and the "RLS Exomars Science" Project (AYA2011-30291-C02-02; Ministry of Science and Innovation, Spain and FEDER funds of EU). We thank the Peñoles Company for allowing access inside the Naica Mine and for support during field work. Logistics was carried out by "NAICA PROJECT" and Speleoresearch and Films of Mexico City in co-operation with La Venta Exploring Team (Italy). Preservation of this unique cave and its speleothems was considered mandatory throughout our investigation and no speleothem was taken from the cave walls. Photographs of Naica caves were kindly provided by La Venta and S/F Archives. Sarah Steines is also acknowledged for improving the English manuscript. Finally, the authors appreciate the suggestions made by Associate Editors Jay Quade and Jaime Urrutia Fucugauchi, Editor Alan Gillespie and two anonymous reviewers, which helped to improve the original manuscript.

References

Allen, B.D., Anderson, R.Y., 2000. A continuous, high resolution record of late Pleistocene climate variability from the Estancia basin, New Mexico. Geological Society of America Bulletin 112, 1444–1458.
Alley, R.B., Mayewski, P.A., Sowers, T., Stuiver, M., Taylor, K.C., Clark, P.U., 1997. Holocene climatic instability: a prominent, widespread event 8200 yr ago. Geology 25, 483–486.
Alva-Valdivia, L.M., Goguitchaichvili, A., Urrutia-Fucugauchi, J., 2003. Petromagnetic properties in the Naica mining district, Chihuahua, Mexico: searching for source of mineralization. Earth, Planets and Space 55, 19–31.
Asmerom, Y., Polyak, V.J., Burn, S.J., 2010. Variable winter moisture in the southwestern United States linked to rapid glacial climate shifts. Nature Geoscience 3, 114–117.
Badino, G., Calaforra, J.M., Forti, P., Garofalo, P., Sanna, L., 2011. The present day genesis and evolution of cave minerals inside the Ojo de la Reina cave (Naica Mine, Mexico). International Journal of Speleology 40 (2), 125–131.
Baker, A., Ito, E., Smart, P.L., McEwan, R.F., 1997. Elevated and variable values of ^{13}C in speleothems in a British cave system. Chemical Geology 136 (3–4), 263–270.
Berenblut, B.J., Dawson, P., Wilkinson, B.R., 1971. The Raman spectrum of gypsum. Spectrochimica Acta Part A 27 (9), 1849–1863.
Bernabei, T., Forti, P., Villasuso, R., 2007. Sails: a new gypsum speleothem from Naica, Chihuahua, Mexico. International Journal of Speleology 26 (1), 23–30.
Beverly, M., Forti, P., 2010. L'esplorazione della Grotta Palacios nella miniera di Naica. Speleologia 63, 46–49.
Bottrell, S.H., Crowley, S.M., Self, C., 2001. Invasion of a karst aquifer by hydrothermal fluids: evidence from stable isotopic compositions of cave mineralization. Geofluids 1, 103–121.
Brook, G.A., Ellwood, B.B., Railsback, L.B., Cowart, J.B., 2006. A 164 ka record of environmental change in the American Southwest from a Carlsbad Cavern speleothem. Palaeogeography, Palaeoclimatology, Palaeoecology 237, 483–507.
Burton, E.A., Walter, L.M., 1987. Relative precipitation rates of aragonite and Mg calcite from seawater: temperature or carbonate ion control? Geology 15, 111–114.
Chávez-Lara, C.M., Roy, P.D., Caballero, M.M., Carreño, A.L., Lakshumanan, C., 2012. Lacustrine ostracodes from the Chihuahuan Desert of Mexico and inferred Late Quaternary paleoecological conditions. Revista Mexicana de Ciencias Geológicas 29, 422–431.
Cortés, A., Durazo, J., Farvolden, R.N., 1997. Studies of isotopic hydrology of the basin of Mexico and vicinity: annotated bibliography and interpretation. Journal of Hydrology 198, 346–376.
de Villiers, S., Greaves, M., Elderfield, H., 2002. An intensity ratio calibration method for the accurate determination of Mg/Ca and Sr/Ca of marine carbonates by ICP-AES. Geochemistry, Geophysics, Geosystems 3, 1–14.
Douglas, M.W., Madox, R.A., Howard, K., 1993. The Mexican monsoon. Journal of Climate 6, 1665–1677.
Erwood, R.J., Kesler, S.E., Cloke, P.L., 1979. Compositionally distinct, saline hydrothermal solutions, Naica Mine, Chihuahua, Mexico. Economic Geology 74, 95–108.
Fairchild, I.J., Smith, C.L., Baker, A., Fuller, L., Spötl, C., Mattey, D., McDermott, F., 2006. Modification and preservation of environmental signals in speleothems. Earth-Science Reviews 75, 105–153.
Fontes, H.C., Gonfiantini, R., 1967. Fractionnement isotopique de l'hydrogene dans l'eau de cristallisation du gypse. Comptes Rendus de l'Académie des Sciences 265, 4–6.
Forti, P., 2003. Un caso evidente di controllo climatico sugli speleotemi: Il moonmilk del Salone Giordani e i "cave raft" del Salone del Fango nella grotta della Spipola (Gessi Bolognesi). Atti 19°Congresso Nazionale di Speleologia, Trieste, pp. 115–126.
Forti, P., 2010. Genesis and evolution of the caves in the Naica mine (Chihuahua, Mexico). Zeitschrift für Geomorphologie 54 (2), 115–135.
Forti, P., Sanna, L., 2010. The Naica project. A multidisciplinary study of the largest gypsum crystal of the world. Episodes 33 (1), 23–32.
Forti, P., Galli, E., Rossi, A., 2008. Il sistema Gesso-Calcite-Aragonite: nuovi dati dalle concrezioni del Livello −590 della Miniera di Naica (Messico). Congresso Nazionale di Speleologia, Iglesias 2007. Memorie dell'IIS s.II, v.21, pp. 139–149.
Foshag, W., 1927. The selenite caves of Naica, Mexico. American Mineralogist 12, 252–256.
Franco-Rubio, M., 1978. Estratigrafía del Albiano-Cenomaniano en la región de Naica, Chihuahua. Revista del Instituto de Geología (México) 2, 132–149.
Frech, R., Wang, E.C., Bates, J.B., 1980. The IR and Raman-spectra of CaCO3 (aragonite). Spectrochimica Acta Part A 36, 915–919.
García-Guinea, J., Morales, S., Delgado, A., Recio, C., Calaforra, J.M., 2002. Formation of gigantic gypsum crystals. Journal of the Geological Society 159, 347–350.
García-Ruiz, J.M., Villasuso, R., Ayora, C., Canals, A., Otálora, F., 2007. Formation of natural gypsum megacrystals in Naica, Mexico. Geology 35 (4), 327–330.
Gardner, G.L., Nancollas, G.H., 1970. Complex formation in lead sulfate solutions. Annals of Chemistry 42 (7), 794–795.
Garofalo, P.S., Fricker, M., Günther, D., Mercuri, A.M., Loreti, M., Forti, P., Capaccioni, B., 2010. A climatic control on the formation of gigantic gypsum crystals within the hypogenic caves of Naica (Mexico). Earth and Planetary Science Letters 289, 560–569.
Gázquez, F., Calaforra, J.M., Forti, P., Rull, F., Martínez-Frías, J., 2012. Gypsum–carbonate speleothems from Cueva de las Espadas (Naica mine, Mexico): mineralogy and palaeohydrogeological implications. International Journal of Speleology 41 (2), 211–220.
Giulivo, I., Mecchia, M., Piccini, P., Sauro, P., 2007. Geology and hydrogeology of Naica. In: Forti, P. (Ed.), Le Grotte di Naica: Esplorazione, documentazione, ricerca. University of Bologna, Bologna, pp. 49–50.
Hardie, L.A., 1967. The gypsum–anhydrite equilibrium at one atmosphere pressure. American Mineralogist 52, 171–200.
Higgins, R.W., Yao, Y., Wang, X.L., 1997. Influence of the North American monsoon system on the U.S. summer precipitation regime. Journal of Climate 10, 2600–2622.
Hodell, D., Turchyn, A.V., Wiseman, C.J., Escobar, J., Curtis, J.H., Brenner, M., Gilli, A., Mueller, A.D., Anselmetti, F., Aritzegui, D., Brown, E., 2012. Late Glacial temperature and precipitation changes in the lowland Neotropics by tandem measurement of δ18O in biogenic carbonate and gypsum hydration water. Geochimica et Cosmochimica Acta 77, 352–368.
Hoefs, J., 2004. Stable Isotope Geochemistry, fifth ed. Springer, New York.
Hoy, R.N., Gross, G.W., 1982. A Baseline Study of Oxygen 18 and Deuterium in the Roswell, New Mexico Groundwater Basin. , 144. New Mexico Water Resources Research Institute 95.
Irving, H.M.N.H., William, R.J.P., 1953. The stability of transition–metal complexes. Journal of the Chemical Society 637, 3192–3210.
Kageyama, M., Combourieu-Nebout, N., Sepulchre, P., Peyron, O., Krinner, G., Ramstein, G., Cazet, J.P., 2005. The Last Glacial Maximum and Heinrich Event 1 in terms of climate and vegetation around the Alboran Sea: a preliminary model-data. Comptes Rendus Geoscience 337, 983–992.
Klemm, L.M., Pettke, T., Heinrich, C.A., 2007. Hydrothermal evolution of the El Teniente deposit, Chile: porphyry Cu–Mo ore deposition from low-salinity magmatic fluids. Economic Geology 102 (6), 1021–1045.
Lachniet, M.S., Asmerom, Y., Burn, S.J., Patterson, W.P., Polyak, V.J., Seltzer, O., 2004. Tropical response to the 8200 yr B.P. cold event? Speleothem isotopes indicate a weakened early Holocene monsoon in Costa Rica. Geology 32, 957–960.
Lauritzen, S.E., Lundberg, J., 1997. TIMS Age4U2U. A program for raw data processing, error propagation and $^{230}Th/^{234}U$ age calculation for mass spectrometry. Turbo Pascal Code. Department of Geology, Bergen University 1856–1885.
Lu, F.H., Meyers, W.J., Schoonen, M.A., 1997. Trace and minor element analyses on gypsum: an experimental study. Chemical Geology 142, 1–10.
Maltsev, V.A., 1997. Minerals of Cupp-Coutunn cave, Cave Minerals of the World, 2nd edition. Natl. Speleol. Soc, Huntsville, AL, pp. 323–328.
Marín-Herrera, R.M., Vorgel, F., Echegoyén, R., 2006. Las megaselenitas del distrito minero de Naica, Chihuahua, una ocurrencia mineralógica anómala. Bulletin de Minéralogie (México) 17, 139–148.
Megaw, P.K.M., Ruiz, J., Titley, S.R., 1988. High-temperature, carbonate-hosted Pb–Zn–Ag (Cu) deposits of northern Mexico. Economic Geology 83, 1856–1885.
Metcalfe, S., Say, A., Black, S., McCulloch, R., O'Hara, S., 2002. Wet conditions during the Last Glaciation in the Chihuahuan Desert, Alta Babicora Basin, Mexico. Quaternary Research 57, 91–101.
Monnin, E., Indermühle, A., Dällenbach, A., Flückinger, J., Stauffer, B., Stocker, T.F., Raynaud, D., Barnola, J.M., 2001. Atmospheric CO_2 concentrations over the last glacial termination. Science 291, 112–114.
Musgrove, M., Banner, J.L., Mack, L., James, E.W., Cheng, H., Edwards, L.R., 2001. Geochronology of the late Pleistocene to Holocene speleothems from central Texas: implications for regional palaeoclimate. Geological Society of America Bulletin 113 (12), 1532–1543.
Onac, B., Forti, P., 2011. Minerogenetic mechanisms occurring in the cave environment: an overview. International Journal of Speleology 40 (2), 79–98.
Patterson, W.P., Smith, G.R., Lohmann, K.C., 1993. Continental paleothermometry and seasonality using the isotopic composition of aragonitic otoliths of freshwater fishes. In: Swart, P.A., Lohmann, K.C., McKenzie, J., Savin, S. (Eds.), Monogr. Continental Climate Change From Isotopic Records. , No. 78. American Geophysical Union, Washington, D.C., pp. 191–202.
Playá, E., Recio, C., Mitchell, J., 2005. Extraction of gypsum hydration water for oxygen isotopic analysis by the guanidine hydrochloride reaction method. Chemical Geology 217, 89–96.

https://doi.org/10.1016/j.yqres.2013.09.004 Published online by Cambridge University Press

Polyak, V.J., Asmerom, Y., Burns, S.J., Lachniet, M.S., 2012. Climatic backdrop to the terminal Pleistocene extinction of North American mammals. Geology 40, 1023–1026.
Pradhananga, T.M., Matsuo, S., 1985. Deuterium/hydrogen fractionation in sulfate hydrate–water systems. Journal of Physical Chemistry 89 (10), 1069–1072.
Richards, D.A., Dorale, J.A., 2003. U-series chronology and environmental applications of speleothems. In: Bourdon, B., Henderson, G.M., Ludstrom, C., Turner, S. (Eds.), Uranium-series geochemistry. Reviews in Mineralogy and Geochemistry, 52, pp. 407–460.
Rickwood, P.C., 1981. The largest crystals. American Mineralogist 66, 885–908.
Rohling, E., Pällke, H., 2005. Centennial-scale climate cooling with a sudden cold event around 8,200 years ago. Nature 434, 975–979.
Roy, P.D., Quiroz-Jiménez, J.D., Pérez-Cruz, L.L., Lozano-García, S., Metcalfe, S.H., Lozano-Santacruz, R., López-Balbiaux, N., Sánchez-Zavala, J.L., Romero, F.M., 2013. Late Quaternary paleohydrological conditions in the drylands of northern Mexico: a summer precipitation proxy record of the last 80 cal ka BP. Quaternary Science Reviews. http://dx.doi.org/10.1016/j.quascirev.2012.11.020 (in press).
Ruiz, J., Barton, M., Palacios, H., 1986. Geology and geochemistry of Naica, Chihuahua Mexico. In: Wisconsin Library Services (Ed.), Lead–Zinc–Silver Carbonate-hosted Deposits of Northern Mexico. A Guidebook for Field Excursions and Mine Work, pp. 169–178.
Rutt, H.N., Nicola, J.H., 1974. Raman spectra of carbonates of calcite structure. Journal of Physical Chemistry Part C Solid State 7, 4522.
Sanna, L., Saez, F., Simonsen, S., Constantin, S., Calaforra, J.M., Forti, P., Lauritzen, S.E., 2010. Uranium-series dating of gypsum speleothems: methodology and examples. International Journal of Speleology 39 (1), 35–46.
Sanna, L., Forti, P., Lauritzen, S.E., 2011. Preliminary U/Th dating and the evolution of gypsum crystals in Naica caves (Mexico). Acta Carsologica 40 (1), 17–28.
Sauer, P.E., Schimmelmann, A., Sessions, A.L., Topalov, K., 2009. Simplified batch equilibration for D/H determination of non-exchangeable hydrogen in solid organic material. Rapid Communications in Mass Spectrometry 23 (7), 949–956.
Shakun, J.D., Carlson, A.E., 2010. A global perspective on the last glacial maximum to Holocene climate change. Quaternary Science Reviews 29, 1801–1816.
Sherman, D.M., 2010. Metal complexation and ion association in hydrothermal fluids: insights from quantum chemistry and molecular dynamics. Geofluids 10 (1–2), 41–57.
Sofer, Z., 1978. Isotopic composition of hydration water in gypsum. Geochimica et Cosmochimica Acta 42, 1141–1149.
Spötl, C., Mangini, A., 2007. Speleothems and paleoglaciers. Earth and Planetary Science Letters 254 (3–4), 323–331.
Van Driessche, A.E.S., García-Ruiz, J.M., Tsukamoto, K., Patiño-López, L.D., Satoh, H., 2011. Ultraslow growth rates of giant gypsum crystals. Proceedings of the National Academy of Sciences of the United States of America 108, 15721.
Yapp, C.J., 1985. D/H variations of meteoric waters in Albuquerque, New Mexico, USA. Journal of Hydrology 76, 63–84.

https://doi.org/10.1016/j.yqres.2013.09.004 Published online by Cambridge University Press